Springtime Arctic ozone depletion forces Northern Hemisphere climate anomalies

Marina Friedel[1,*], Gabriel Chiodo[1,2], Andrea Stenke[1,3,4], Daniela I.V. Domeisen[5,1], Stephan Fueglistaler[6,7], Julien Anet[8], and Thomas Peter[1]

[1]ETH Zürich, Institute for Atmospheric and Climate Science, Zürich, Switzerland

[2]Applied Physics and Applied Math, Columbia University, NY, USA

[3]ETH Zürich, Institute of Biogeochemistry and Pollutant Dynamics, Zürich, Switzerland

[4]Eawag, Swiss Federal Institute of Aquatic Science and Technology, Dübendorf, Switzerland

[5]University of Lausanne, Lausanne, Switzerland

[6]Department of Geosciences, Princeton University, Princeton, NJ, USA

[7]Program in Atmospheric and Oceanic Sciences, Princeton University, Princeton, NJ, USA

[8]ZHAW, School of Engineering, Winterthur, Switzerland

[*]marina.friedel@env.ethz.ch

Abstract

Large-scale chemical depletion of ozone due to anthropogenic emissions occurs over Antarctica as well as, to a lesser degree, the Arctic. Surface climate predictability in the Northern Hemisphere might be improved due to a previously proposed, albeit uncertain, link to springtime ozone depletion in the Arctic. Here, we use observations and targeted chemistry-climate experiments from two models to isolate the surface impacts of ozone depletion from complex downward dynamical influences. We find that springtime stratospheric ozone depletion is consistently followed by surface temperature and precipitation anomalies with signs consistent with a positive Arctic Oscillation, namely warm and dry conditions over southern Europe and Eurasia and moistening over northern Europe. Notably, we show that these anomalies, affecting large portions of the Northern Hemisphere, are substantially driven by the loss of stratospheric ozone. This is likely due to ozone depletion leading to a reduction in shortwave radiation absorption, when in turn causing persistent negative temperature anomalies in the lower stratosphere and a delayed breakup of the polar vortex. These results indicate that the inclusion of interactive ozone chemistry in atmospheric models can considerably improve the predictability of Northern Hemisphere surface climate on seasonal timescales.

In the Southern Hemisphere (SH), polar stratospheric ozone has declined drastically since the late 1970s due to anthropogenic emissions of gases such as chlorofluorocarbons (CFCs) and bromine-containing halons, resulting in the yearly formation of an ozone hole over the Antarctic in austral spring [1]. This decrease in ozone is not only critical for human health and ecosystems [2, 3], but has been linked to large-scale climatic changes in the SH [4, 5, 6, 7]. While long-term changes in SH surface climate have been clearly attributed to radiative and dynamical impacts of Antarctic ozone depletion [8], recent studies also show a clear connection between the state of the Antarctic ozone layer in spring and subsequent surface climate on seasonal timescales [6, 9, 10].

Owing to stronger planetary wave fluxes in the Northern Hemisphere (NH), which result in increased transport of ozone-rich air into the polar regions and less favorable conditions for ozone

depletion compared to the SH, the observed relative trend in Arctic stratospheric ozone is much smaller than over the Antarctic. Yet, drastic springtime ozone losses with magnitudes typical for the Antarctic can also occur in the Arctic stratosphere, most recently in spring 2020 [11, 12]. Observations and model simulations suggest that such low springtime Arctic ozone concentrations are followed by surface anomalies resembling a positive phase of the Arctic Oscillation (AO) [13, 14], consistent with observations in the SH. Some analyses argue that this ozone-surface climate connection could be useful for statistical and model predictions [15, 16] of NH climate.

However, it remains difficult to disentangle the potential downward influence of ozone extremes from extreme dynamical events in the stratosphere, for which a surface impact is well established [17, 18, 19]. Surface patterns coincident with ozone depletion might be caused entirely by dynamical variability in the lower stratosphere, with ozone simply acting as a passive tracer of such dynamical variability [20, 21]. Conversely, some studies based on models and observations conclude that ozone extremes actively influence surface climate [14, 13]. Inconclusive results arise from both a lack of model studies which explicitly isolate the ozone feedbacks, and the specific analysis methods used in past studies. Until now, there is neither robust evidence for a causal link between springtime stratospheric ozone and NH surface climate, nor has the impact of ozone feedbacks been quantitatively assessed. Moreover, past studies focused on monthly averaged climate variables and chose fixed reference months (March/April) to define springtime ozone extremes, ignoring inter-annual variations in the timing of those events.

Many operational forecast and reanalysis systems as well as climate models neglect possible impacts of stratospheric ozone on surface climate by prescribing a diagnostic ozone forcing [22, 23, 24], thus ignoring ozone feedbacks. Furthermore, they typically use a zonally averaged ozone climatology, whereas a longitudinally resolved ozone forcing may better represent the climatology and trends of the Arctic polar vortex and surface climate, as idealized model experiments show [25, 26, 27]. However, the importance of the spatial structure during Arctic ozone depletion is still unclear. A three-dimensional representation of stratospheric ozone in prediction models could therefore help to improve predictability at the surface.

Here, we shed new light on the surface impacts of Arctic ozone depletion by (1) improving

the detection of ozone depletion events and their surface signature through consideration of their relative timing and by (2) disentangling effects of ozone feedbacks, zonal ozone asymmetries and dynamical contributions in model simulations.

Ozone-surface climate connection in observations

We revisit springtime ozone depletion and associated surface patterns from 1980 to 2020 in the MERRA2 reanalysis dataset [28]. We define springtime ozone minima based on partial stratospheric ozone column (30-70 hPa) over the polar cap (60-90°N) and identify and rank for each year the minima in daily ozone values within March and April, and the day exhibiting the lowest ozone value is termed as "ozone minimum date". In the following, we use the terms "ozone minima" and "ozone depletion" interchangeably (see section S5). For further analysis, the 10 years — 25% of the 41 year-long period — with the lowest springtime ozone values are considered. This detection method allows for a better alignment of stratospheric ozone depletion and associated surface effects compared to previous studies [14, 13].

In the 30 days following the ozone minimum date, we find predominantly a positive phase of the AO (Fig. 2, mean AO index of 0.52) with negative sea level pressure (SLP) anomalies in the polar region and positive SLP anomalies in midlatitudes, especially over northwestern Europe (Fig. 1 a). This pattern is consistent with previous studies [13]. The positive AO is associated with regional temperature anomalies; warming over Siberia and large parts of Eurasia (up to 2 K) as well as over western Europe (up to 1 K), and cooling over southeastern Europe (Fig. 1 b). Furthermore, we find reduced precipitation over large parts of Europe and central Asia, and increased precipitation over the Arctic (Fig. 1 c).

Even though MERRA2 shows a strong connection between stratospheric ozone depletion and a positive AO at the surface, the spread in the mean AO index averaged over the month after the ozone minimum date between individual events is large, and for 2 out of the 10 events the AO is negative (Fig. 2). This spread is similar to the uncertainty in the tropospheric response after Sudden Stratospheric Warmings (SSWs) [29, 30]. Nevertheless, there is a clear shift towards a predominantly positive phase of the AO in the aftermath of stratospheric ozone depletion. Our new

detection method used here not only confirms the robust statistical connection between springtime stratospheric ozone values and surface climate reported previously, but also reveals an even larger surface signal following strong stratospheric ozone depletion than reported by past studies[14, 13] (see Fig. S9).

Isolating the influence of ozone on surface climate

In order to establish the causality of the ozone-surface coupling, we perform targeted model experiments designed to isolate the ozone impact on stratospheric dynamics and surface climate, known as ozone feedbacks. We use two chemistry-climate-models, WACCM4 [31] and SOCOL-MPIOM [32]. These models have different dynamical cores and chemistry modules, offering independent responses. With both models, we perform three simulations employing present-day boundary conditions: one with fully interactive ozone chemistry (INT-3D), one with prescribed daily three-dimensional climatological ozone (CLIM-3D), and one with a prescribed zonally averaged ozone climatology (CLIM-2D) from the same underlying model to avoid introducing any systematic biases. Unlike other studies using a similar set-up [27, 33], experiments with prescribed ozone climatologies (CLIM-3D and CLIM-2D) still employ the chemistry scheme. However, in these experiments, the calculated ozone field is radiatively inactive — instead, the respective ozone climatology is used by the radiation module. Thus, the calculated ozone purely acts as a passive tracer in CLIM-3D and CLIM-2D and ozone feedbacks on the atmospheric circulation are disabled (see Fig. 3 a).

Simulations with WACCM using a climatological zonal mean ozone field (CLIM-2D) show significant negative SLP anomalies over the polar cap, positive temperature anomalies over large parts of Eurasia and increased precipitation close to the pole following the 25% strongest springtime ozone minima (Fig. 1 j-l). Surface anomalies in CLIM-2D following Arctic ozone depletion are thus comparable to observations in their sign and pattern for large parts of the NH, but are substantially weaker (cp. to Fig. 1 a-c). Simulations employing a three-dimensional ozone climatology (CLIM-3D) show slightly improved results compared to the observations, especially over Europe. The CLIM-3D experiment captures the observed high SLP and temperature anomalies as well as dry

anomalies over northwestern Europe: this pattern is absent in CLIM-2D (Fig. 1 g-l). However, neither CLIM-2D nor CLIM-3D captures the full magnitude of the surface signal (i.e. they only capture up to 40% of the AO signal in WACCM). Since ozone anomalies do not exert any radiative-dynamical feedback in the CLIM setting, springtime surface anomalies in these runs are solely due to dynamical variability, and are linked to an exceptionally strong polar vortex and a cold stratosphere. This suggests that the magnitude of surface patterns found in the observations cannot be explained by dynamical variability alone.

Simulations with interactive ozone (INT-3D), which additionally include ozone feedbacks, show significantly enhanced surface anomalies compared to CLIM-2D and CLIM-3D in the 30 days after springtime Arctic ozone depletion. More specifically, negative SLP anomalies over the pole are up to 4 hPa larger (Fig. 1 d), temperature anomalies in Eurasia are enhanced by more than 1 K (Fig. 1 e) and precipitation anomalies over the Arctic are increased (Fig. 1 f). Most notably, the distribution of the AO index and its mean (0.50) in the month after the ozone minimum date in INT-3D is comparable to the AO index in reanalysis with a mean of 0.52, while the mean is smaller in CLIM-3D (0.21) and close to zero in CLIM-2D (0.01) (Fig. 2). Since differences in surface anomalies between INT-3D and CLIM show the direct impact of ozone feedbacks, we conclude that stratospheric ozone actively forces NH surface climate in the aftermath of springtime ozone depletion.

Model experiments with SOCOL-MPIOM corroborate these results, albeit with a slightly smaller ozone impact. In SOCOL-MPIOM, anomalies in surface temperature are weaker in CLIM-2D compared to INT-3D, while in simulations with a three-dimensional ozone climatology (CLIM-3D) the anomalies are well captured for some parts of the Northern Hemisphere, especially over Europe and Siberia (see Extended Data Figure 1). However, zonal asymmetries both in the ozone distribution and in the polar vortex are overestimated by this model (Figs. S3, S4, S5), which might lead to an overestimation of the surface impact of ozone asymmetries (CLIM-3D vs. CLIM-2D). The impact of zonal asymmetries of a climatological ozone forcing is thus model dependent (see supplementary material). In addition, the magnitude of the AO response is to some extent model dependent. Whereas there is a strong (60%) and significant enhancement of the AO induced by

ozone anomalies in WACCM, the signal in SOCOL-MPIOM is smaller (30%) and less significant (see Fig. S2). However, the AO index in SOCOL-MPIOM is less congruent with the SLP anomalies around the ozone minima than in WACCM (see Extended Data Figure 2, Fig. S1). Hence, the AO index does not reflect the full extent of the ozone-induced surface patterns in SOCOL-MPIOM. Despite these caveats, the contribution of ozone depletion to regional surface anomalies is consistent across models is: in both models, ozone feedbacks substantially contribute to certain features of the surface signal, such as the low pressure anomaly over the North pole and the high pressure anomaly and decreased precipitation over Northern Europe (Extended Data Figures 5, 6). The robustness of these results in both models emphasizes the importance of interactive ozone chemistry to capture the full magnitude of the surface signal following Arctic ozone depletion.

Ozone feedback mechanism

Comparison of stratospheric conditions in CLIM and INT-3D experiments around the ozone minima provides insights into the mechanism through which ozone affects surface climate. Impacts of ozone asymmetries on the polar vortex shape are discussed in the supplementary material (Figs. S3, S4, S5). Ozone depletion is closely tied to a strong stratospheric vortex with a cold lower stratosphere [34]. This strong polar vortex is generally accompanied by positive temperature anomalies in the upper stratosphere [35, 36] due to increased wave guiding towards and increased dissipation within the upper stratosphere. These upper stratosphere temperature anomalies descend to the lower stratosphere once sunlight returns to the polar cap in spring and the vortex starts to dissipate; this is reproduced by all model experiments (see Fig. 5 a for WACCM (contour lines), and Extended Data Figure 4 c, d for SOCOL-MPIOM). In the lower stratosphere, a stronger polar vortex is associated with reduced transport of ozone-rich air into the polar regions [33], which contributes dynamically to the reduced Arctic ozone abundance.

Ozone depletion by anthropogenic halogens initiated by these background conditions exerts an additional forcing on stratospheric temperature and dynamics: due to the loss of ozone, there is less solar absorption in the stratosphere between 50-100 hPa in model simulations that include ozone feedbacks (Fig. 5 c), leading to larger and more persistent cold anomalies in the lower stratosphere

(see Fig. 5 a). As a result, the depletion event prolongs the lifetime of the polar vortex. In model experiments including ozone feedbacks, the spring polar vortex breakup ("final warming") is significantly delayed compared to experiments with climatological ozone (by up to 10 days, see Table S1). Hence, Arctic ozone anomalies actively extend stratospheric winter conditions, which is expressed by a more persistent positive Northern Annular Mode (NAM) index in the lower stratosphere in INT-3D compared to CLIM (Fig. 4). Prolonged stratospheric anomalies are expected to induce anomalous states in the troposphere and a shift in the surface AO [29], which is evident in WACCM (see Fig. 2). In SOCOL-MPIOM, the lower stratospheric anomalies (i.e. NAM at 100 hPa) are sustained and coupling to the troposphere is enhanced (see Extended Data Figures 3, 4), although less than in WACCM. Since the lifetime of stratospheric anomalies is critically related to the magnitude of their surface response [37], the less persistent polar vortex in SOCOL-MPIOM might reduce the AO response in this model compared to WACCM.

Moreover, positive temperature anomalies in the upper and middle stratosphere are stronger in simulations including ozone feedbacks (Fig. 5 a, days 30-60). This is due to an increase in planetary wave dissipation following the strengthening of the polar vortex through ozone feedbacks, similar to what has been reported previously for spring conditions with an already weakened polar vortex [38, 39, 27]. An increase in planetary wave breaking in the upper stratosphere leads to a strengthening of the Brewer-Dobson circulation (BDC), which implies increased downwelling over the pole, resulting in adiabatic heating [38] (Fig. 5 d, days 30-60).

A schematic illustration of the ozone feedback mechanism is shown in Figure 3 b. The ozone feedback mechanism presented here is the first description of the downward impact of springtime ozone depletion in the NH in a mechanistic way and is consistent with our understanding of the dynamical impacts of the ozone hole in the SH. Even though ozone depletion is much less frequent in the Arctic than in the Antarctic, we conclude that the large contribution of ozone depletion to springtime surface climate as well as the mechanism by which ozone affects the stratospheric circulation is analogous in both hemispheres.

Implications for predictability

Dynamical variability in the stratosphere has previously been shown to provide skill for subseasonal to seasonal prediction for the Northern Hemisphere, both for winter (e.g., refs. [40, 41, 42]) and for spring [43]. Such stratospheric predictability bears a broad societal relevance, for example in the context of wind electricity generation [44] and human health [45]. Forecast systems with an enhanced stratospheric resolution have been shown to provide improved skill for tropospheric predictions [46]. Forecast errors for the North Atlantic region can be traced back to the initial state of the polar stratospheric vortex and uncertainties in stratosphere-troposphere coupling in a sub-seasonal prediction system [47]. One potential reason for such errors is that most state-of-the-art prediction systems lack interactive stratospheric ozone chemistry [48]. Indeed, stratospheric ozone information could further enhance sub-seasonal to seasonal predictions, and experiments with a simplified ozone scheme that mimics interactions between dynamics and chemistry show promising results [16].

The results presented here contribute to this discussion in two ways: First, they shed new light on the nature of the ozone-surface climate connection in the NH — a relationship controversially discussed. Our modelling experiments show in a robust manner that the substantial fraction of the springtime NH surface pattern in the aftermath of strong stratospheric ozone depletion cannot be explained by dynamical variability alone. Rather, ozone feedbacks represent an important contribution to the surface response. We therefore conclude that interactive ozone chemistry is essential for weather and climate models to realistically reproduce NH spring conditions. Where interactive ozone chemistry is not feasible, our results suggest that a spatially resolved ozone forcing can lead to improvements compared to the method still widely used in weather and climate prediction, namely a zonally averaged ozone representation [22, 23, 24]. However, impacts of ozone asymmetries are model-dependent and stratosphere-troposphere coupling is highly underestimated when interactive ozone chemistry is absent (Fig. 4, Extended Data Figure 3). A second contribution is that these novel findings create new incentives to explore the value of stratospheric ozone for subseasonal to seasonal prediction. Our results should thus serve as a motivation to explore ways

to include a more realistic representation of stratospheric ozone in forecast models, and to further investigate the prediction skill arising from stratospheric ozone depletion in current and future climate for both hemispheres. Despite the projected Arctic ozone recovery, large dynamical variability will ensue in the future, leading to large episodic springtime depletion [49]. Hence, Arctic ozone will continue playing an important role in future climate variability.

Acknowledgements

We are grateful for the assistance from U. Beyerle in data management and thank S. Muthers for support in the chemistry-climate modelling with SOCOL-MPIOM. Support from the Swiss National Science Foundation through Ambizione Grant PZ00P2_180043 for M.F. and G.C, and projects PP00P2_170523 and PP00P2_198896 to D.D. is gratefully acknowledged.

Author contributions

G.C. conceived the modelling experiments, G.C., M.F., A.S. and J.A. conducted the modelling experiments, M.F. and G.C. processed the data, M.F., G.C., T.P., D.D. and S.F. analysed and interpreted the results. M.F. wrote the paper with input from all authors.

Competing interests

The authors declare no competing interests.

Additional information

Supplementary information is available for this study.

Correspondance and request for materials

should be directed to Marina Friedel (marina.friedel@env.ethz.ch).

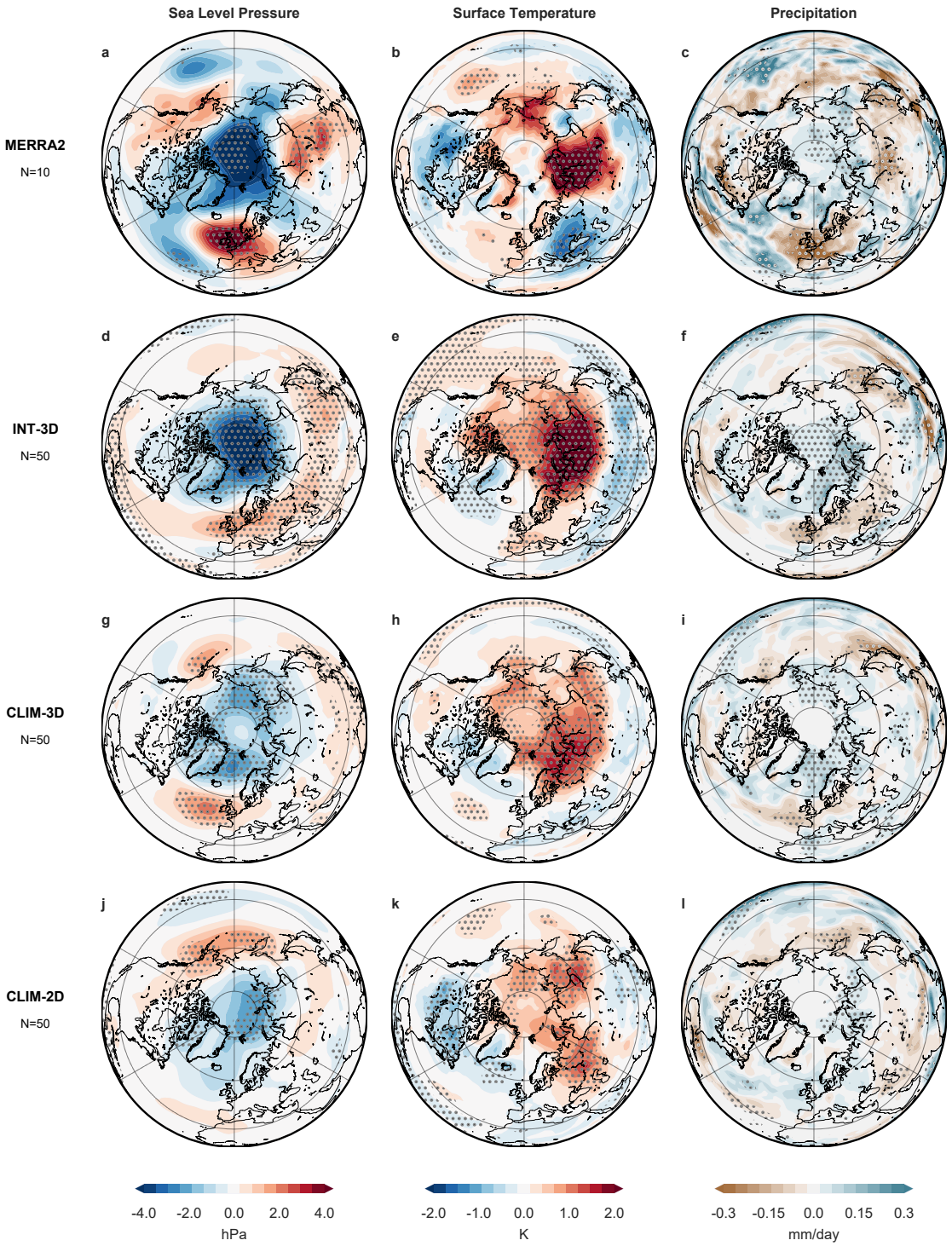

Figure 1. Surface climate following springtime Arctic ozone depletion. Composites of sea level pressure (a, d, g,j), surface temperature (b, e, h, k) and precipitation (c, f, i, l) anomalies in observations (top row), WACCM INT-O3 (second row), CLIM-3D (third row) and CLIM-2D (bottom row) after ozone minima in the 25% of winters with most extreme ozone loss (average over the 30 days after the ozone minimum date). Stippling shows significance on a 4.6% level (2 $\cdot\sigma$) following a bootstrapping test. The following springs are included in the observations (top row): 2020, 2011, 2005, 2002, 2000, 1997, 1996, 1995, 1993, 1990.

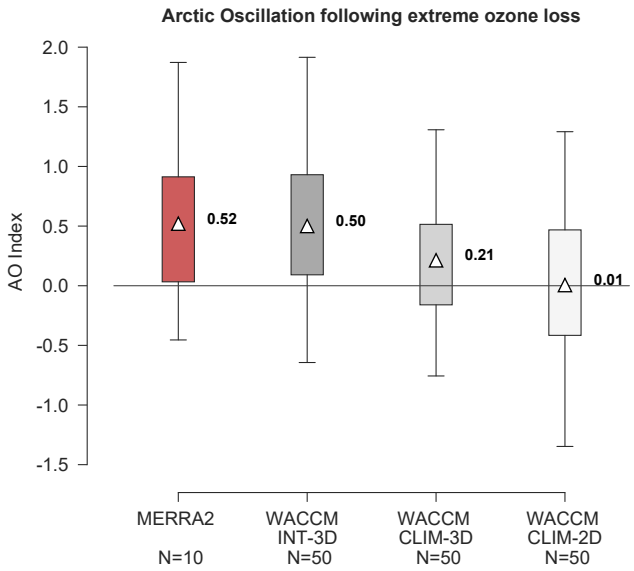

Figure 2. The Arctic Oscillation index following winters with extreme ozone loss in the month after the ozone minimum date. The box plot shows the distribution of the mean AO index (20 - 90°N) at 1000 hPa in the month following the ozone minimum for MERRA2 (red) and WACCM (grey) INT-O3, CLIM-O3 and CLIM-2D. Triangles and numbers indicate the mean Arctic Oscillation index in the month after the ozone minimum date averaged over the 25% most extreme winters. The upper and lower edges of the boxes show the upper and lower quartile, the whiskers represent the maximum and minimum values of the respective distribution. For MERRA2, individual data points for each ozone minimum are shown. For a discussion of the robustness of the AO response, refer to section S2.

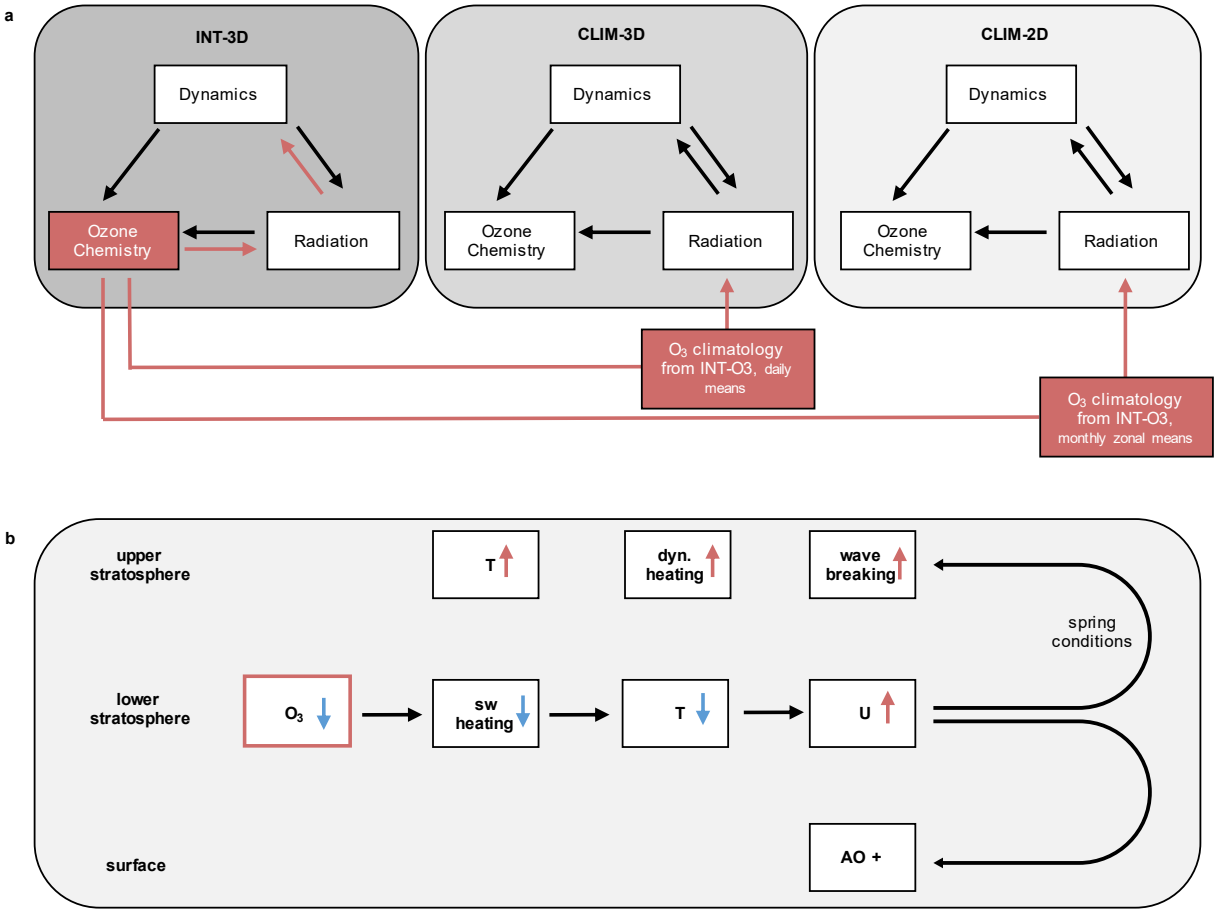

Figure 3. Simulation setup and ozone feedback mechanism. (a) Setup of the simulations with interactive ozone (INT-3D), prescribed three-dimensional climatological ozone (CLIM-3D) and prescribed monthly zonal mean climatological ozone (CLIM-2D). INT-3D treats ozone chemistry fully interactively, i.e. the calculated ozone field has a direct feedback on the atmosphere via the model radiation schemes. In contrast, the CLIM experiments do not use interactively calculated ozone in the radiation module. Instead, the radiation module uses an ozone climatology, which has been derived from INT-3D runs with interactive ozone of the same model. (b) Ozone feedback mechanism in the aftermath of strong springtime Arctic ozone loss. Shown are impacts of ozone depletion on short wave (sw) heating, temperature, and wind speed in the lower stratosphere and subsequent impacts on surface AO and upper stratospheric temperature.

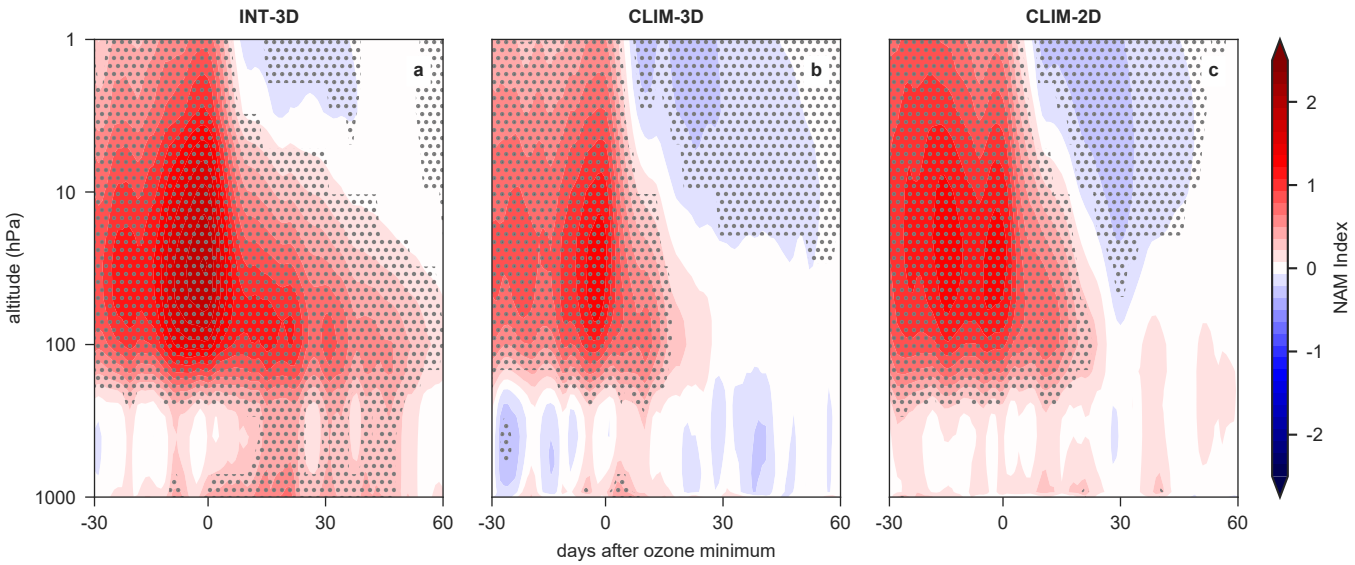

Figure 4. Influence of ozone depletion on stratosphere-troposphere coupling. Composites of Northern Annular Mode (NAM) indices (20 - 90°N) around the ozone minima in WACCM INT-3D (a), CLIM-3D (b) and CLIM-2D (c). Day zero indicates the date with the largest extent of the ozone minima ("ozone minimum date"). Stippling shows significance on a 4.6% ($2 \cdot \sigma$) level following a bootstrapping test (see methods).

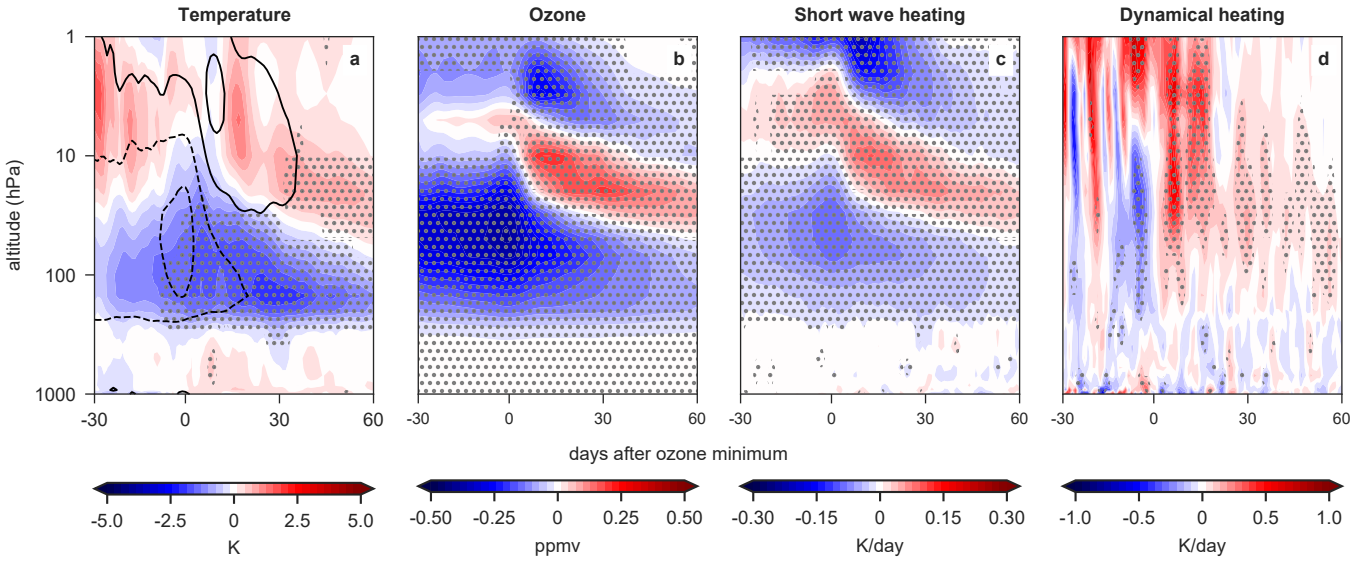

Figure 5. Impact of ozone feedbacks on shortwave and dynamical heating. Differences of polar cap (60-90°N) temperature (a), ozone (b), shortwave heating (c) and dynamical heating (d) anomalies between INT-3D and CLIM-3D around the ozone minima in WACCM. Day zero indicates the date with the largest extent of the ozone minima ("ozone minimum date"). Contour lines in the temperature plot show temperature anomalies in CLIM-2D around the ozone minima with a contour interval of 1.5 K. Stippling shows significance on a 4.6% ($2 \cdot \sigma$) level following a bootstrapping test.

References

[1] Solomon, S. Stratospheric ozone depletion: A review of concepts and history. *Rev. Geophys.* **37**, 275–316, DOI: https://doi.org/10.1029/1999RG900008 (1999).

[2] Henriksen, T., Dahlback, A., Larsen, S. H. & Moan, J. Ultraviolet-radiation and skin cancer. effect of an ozone layer depletion. *Photochem. Photobiol.* **51**, 579–582, DOI: https://doi.org/10.1111/j.1751-1097.1990.tb01968.x (1990).

[3] Ballaré, C. L. *et al.* Impacts of solar ultraviolet-B radiation on terrestrial ecosystems of Tierra del Fuego (southern Argentina): An overview of recent progress. *J. Photochem. Photobiol. B: Biol.* **62**, 67–77, DOI: https://doi.org/10.1016/S1011-1344(01)00152-X (2001).

[4] Gillett, N. P. & Thompson, D. W. J. Simulation of Recent Southern Hemisphere Climate Change. *Science* **302**, 273–275, DOI: 10.1126/science.1087440 (2003).

[5] Thompson, D. W. J. & Solomon, S. Interpretation of Recent Southern Hemisphere Climate Change. *Science* **296**, 895–899, DOI: 10.1126/science.1069270 (2002).

[6] Bandoro, J., Solomon, S., Donohoe, A., Thompson, D. W. J. & Santer, B. D. Influences of the Antarctic Ozone Hole on Southern Hemispheric Summer Climate Change. *J. Clim.* **27**, 6245 – 6264, DOI: 10.1175/JCLI-D-13-00698.1 (2014).

[7] Dennison, F., Mcdonald, A. & Morgenstern, O. The effect of ozone depletion on the Southern Annular Mode and stratosphere-troposphere coupling. *J. Geophys. Res. Atmospheres* **120**, DOI: 10.1002/2014JD023009 (2015).

[8] Thompson, D. *et al.* Signatures of the Antarctic ozone hole in Southern Hemisphere surface climate change. *Nat. Geosci.* **4**, 741–749, DOI: 10.1038/ngeo1296 (2011).

[9] Gillett, Z. E. *et al.* Evaluating the Relationship between Interannual Variations in the Antarctic Ozone Hole and Southern Hemisphere Surface Climate in Chemistry–Climate Models. *J. Clim.* **32**, 3131 – 3151, DOI: 10.1175/JCLI-D-18-0273.1 (2019).

[10] Son, S.-W., Purich, A., Hendon, H. H., Kim, B.-M. & Polvani, L. M. Improved seasonal forecast using ozone hole variability? *Geophys. Res. Lett.* **40**, 6231–6235, DOI: https://doi.org/10.1002/2013GL057731 (2013).

[11] Lawrence, Z. D. *et al.* The Remarkably Strong Arctic Stratospheric Polar Vortex of Winter 2020: Links to Record-Breaking Arctic Oscillation and Ozone Loss. *J. Geophys. Res. Atmospheres* **125**, e2020JD033271, DOI: https://doi.org/10.1029/2020JD033271 (2020).

[12] Manney, G. L. *et al.* Record-Low Arctic Stratospheric Ozone in 2020: MLS Observations of Chemical Processes and Comparisons With Previous Extreme Winters. *Geophys. Res. Lett.* **47**, e2020GL089063, DOI: https://doi.org/10.1029/2020GL089063 (2020).

[13] Ivy, D. J., Solomon, S., Calvo, N. & Thompson, D. W. J. Observed connections of Arctic stratospheric ozone extremes to Northern Hemisphere surface climate. *Environ. Res. Lett.* **12**, 024004, DOI: 10.1088/1748-9326/aa57a4 (2017).

[14] Calvo, N., Polvani, L. M. & Solomon, S. On the surface impact of Arctic stratospheric ozone extremes. *Environ. Res. Lett.* **10**, 094003, DOI: 10.1088/1748-9326/10/9/094003 (2015).

[15] Stone, K. A., Solomon, S., Kinnison, D. E., Baggett, C. F. & Barnes, E. A. Prediction of Northern Hemisphere Regional Surface Temperatures Using Stratospheric Ozone Information. *J. Geophys. Res. Atmospheres* **124**, 5922–5933, DOI: https://doi.org/10.1029/2018JD029626 (2019).

[16] Monge-Sanz, B. M. *et al.* A stratospheric prognostic ozone for seamless Earth System Models: performance, impacts and future. *Atmospheric Chem. And Phys.* 1–39, DOI: 10.5194/acp-2020-1261 (2021).

[17] Ayarzagüena, B. & Serrano, E. Monthly Characterization of the Tropospheric Circulation over the Euro-Atlantic Area in Relation with the Timing of Stratospheric Final Warmings. *J. Clim.* **22**, 6313 – 6324, DOI: 10.1175/2009JCLI2913.1 (2009).

[18] Black, R. X. & McDaniel, B. A. The Dynamics of Northern Hemisphere Stratospheric Final Warming Events. *J. Atmospheric Sci.* **64**, 2932 – 2946, DOI: 10.1175/JAS3981.1 (2007).

[19] Domeisen, D. I. V. & Butler, A. H. Stratospheric drivers of extreme events at the Earth's surface. *Commun. Earth & Environ.* **1**, 59, DOI: 10.1038/s43247-020-00060-z (2020).

[20] Harari, O. *et al.* Influence of Arctic stratospheric ozone on surface climate in CCMI models. *Atmospheric Chem. Phys.* **19**, 9253–9268, DOI: 10.5194/acp-19-9253-2019 (2019).

[21] Rao, J. & Garfinkel, C. I. Arctic Ozone Loss in March 2020 and its Seasonal Prediction in CFSv2: A Comparative Study With the 1997 and 2011 Cases. *J. Geophys. Res. Atmospheres* **125**, e2020JD033524, DOI: https://doi.org/10.1029/2020JD033524 (2020).

[22] Hersbach, H. *et al.* The ERA5 global reanalysis. *Q. J. Royal Meteorol. Soc.* **146**, 1999–2049, DOI: https://doi.org/10.1002/qj.3803 (2020).

[23] Eyring, V. *et al.* Long-term ozone changes and associated climate impacts in CMIP5 simulations. *J. Geophys. Res. Atmospheres* **118**, 5029–5060, DOI: https://doi.org/10.1002/jgrd.50316 (2013).

[24] Cionni, I. *et al.* Ozone database in support of CMIP5 simulations: Results and corresponding radiative forcing. *Atmos. Chem. Phys.* **11**, 11267–11292, DOI: 10.5194/acp-11-11267-2011 (2011).

[25] McCormack, J. P., Nathan, T. R. & Cordero, E. C. The effect of zonally asymmetric ozone heating on the northern hemisphere winter polar stratosphere. *Geophys. Res. Lett.* **38**, DOI: https://doi.org/10.1029/2010GL045937 (2011).

[26] Zhang, J. *et al.* The Influence of Zonally Asymmetric Stratospheric Ozone Changes on the Arctic Polar Vortex Shift. *J. Clim.* **33**, 4641 – 4658, DOI: 10.1175/JCLI-D-19-0647.1 (2020).

[27] Haase, S. & Matthes, K. The importance of interactive chemistry for stratosphere-troposphere coupling. *Atmospheric Chem. Phys.* **19**, 3417–3432, DOI: 10.5194/acp-19-3417-2019 (2019).

[28] Gelaro, R. *et al.* The Modern-Era Retrospective Analysis for Research and Applications, Version 2 (MERRA-2). *J. Clim.* **30**, 5419 – 5454, DOI: 10.1175/JCLI-D-16-0758.1 (2017).

[29] Baldwin, M. P. & Dunkerton, T. J. Stratospheric Harbingers of Anomalous Weather Regimes. *Science* **294**, 581–584, DOI: 10.1126/science.1063315 (2001).

[30] Domeisen, D. I. Estimating the Frequency of Sudden Stratospheric Warming Events From Surface Observations of the North Atlantic Oscillation. *J. Geophys. Res. Atmospheres* **124**, 3180–3194, DOI: https://doi.org/10.1029/2018JD030077 (2019).

[31] Marsh, D. R. *et al.* Climate Change from 1850 to 2005 Simulated in CESM1(WACCM). *J. Clim.* **26**, 7372 – 7391, DOI: 10.1175/JCLI-D-12-00558.1 (2013).

[32] Muthers, S. *et al.* The coupled atmosphere–chemistry–ocean model SOCOL-MPIOM. *Geosci. Model. Dev.* **7**, 2157–2179, DOI: 10.5194/gmd-7-2157-2014 (2014).

[33] Oehrlein, J., Chiodo, G. & Polvani, L. M. The effect of interactive ozone chemistry on weak and strong stratospheric polar vortex events. *Atmospheric Chem. Phys.* **20**, 10531–10544, DOI: 10.5194/acp-20-10531-2020 (2020).

[34] Solomon, S., Garcia, R., Rowland, F. & Wuebbles, D. On the Depletion of Antarctic Ozone. *Nature* **321**, 755–758, DOI: 10.1038/321755a0 (1986).

[35] Kuroda, Y. & Kodera, K. Variability of the polar night jet in the Northern and Southern Hemispheres. *J. Geophys. Res. Atmospheres (1984 - 2012)* **106**, 20703–20713, DOI: https://doi.org/10.1029/2001JD900226 (2001).

[36] Kuroda, Y. & Kodera, K. Role of the Polar-night Jet Oscillation on the formation of the Arctic Oscillation in the Northern Hemisphere winter. *J. Geophys. Res. Atmospheres* **109**, DOI: https://doi.org/10.1029/2003JD004123 (2004).

[37] Runde, T., Dameris, M., Garny, H. & Kinnison, D. E. Classification of stratospheric extreme events according to their downward propagation to the troposphere. *Geophys. Res. Lett.* **43**, 6665–6672, DOI: https://doi.org/10.1002/2016GL069569 (2016).

[38] Charney, J. G. & Drazin, P. G. Propagation of planetary-scale disturbances from the lower into the upper atmosphere. *J. Geophys. Res. (1896-1977)* **66**, 83–109, DOI: https://doi.org/10.1029/JZ066i001p00083 (1961).

[39] Lin, P. *et al.* Dependence of model-simulated response to ozone depletion on stratospheric polar vortex climatology. *Geophys. Res. Lett.* **44**, 6391–6398, DOI: https://doi.org/10.1002/2017GL073862 (2017).

[40] Butler, A. *et al.* Chapter 11 - Sub-seasonal Predictability and the Stratosphere. In Robertson, A. W. & Vitart, F. (eds.) *Sub-Seasonal to Seasonal Prediction*, 223–241, DOI: https://doi.org/10.1016/B978-0-12-811714-9.00011-5 (Elsevier, 2019).

[41] Nie, Y. *et al.* Stratospheric initial conditions provide seasonal predictability of the North Atlantic and Arctic Oscillations. *Environ. Res. Lett.* **14**, 034006, DOI: 10.1088/1748-9326/ab0385 (2019).

[42] Domeisen, D. I. V. *et al.* The Role of the Stratosphere in Subseasonal to Seasonal Prediction: 2. Predictability Arising From Stratosphere-Troposphere Coupling. *J. Geophys. Res.* **125**, 1–20, DOI: https://doi.org/10.1029/2019JD030923 (2020).

[43] Butler, A. H., Perez, A. C., Domeisen, D. I. V., Simpson, I. R. & Sjoberg, J. Predictability of Northern Hemisphere Final Stratospheric Warmings and Their Surface Impacts. *Geophys. Res. Lett.* **43**, 23, DOI: https://doi.org/10.1029/2019GL083346 (2019).

[44] Beerli, R., Wernli, H. & Grams, C. M. Does the lower stratosphere provide predictability for month-ahead wind electricity generation in Europe? *Q. J. Royal Meteorol. Soc.* **143**, 3025–3036, DOI: https://doi.org/10.1002/qj.3158 (2017).

[45] Charlton-Perez, A. J., Aldridge, R. W., Grams, C. M. & Lee, R. Winter pressures on the UK health system dominated by the Greenland Blocking weather regime. *Weather. Clim. Extrem.* **25**, 100218, DOI: https://doi.org/10.1016/j.wace.2019.100218 (2019).

[46] Butler, A. H. *et al.* The Climate-system Historical Forecast Project: do stratosphere-resolving models make better seasonal climate predictions in boreal winter? *Q. J. Royal Meteorol. Soc.* **142**, 1413–1427, DOI: https://doi.org/10.1002/qj.2743 (2016).

[47] Kolstad, E. W., Wulff, C. O., Domeisen, D. I. V. & Woollings, T. Tracing North Atlantic Oscillation Forecast Errors to Stratospheric Origins. *J. Clim.* **33**, 9145 – 9157, DOI: 10.1175/JCLI-D-20-0270.1 (2020).

[48] Domeisen, D. I. *et al.* The Role of the Stratosphere in Subseasonal to Seasonal Prediction: 1. Predictability of the Stratosphere. *J. Geophys. Res. Atmospheres* **125**, e2019JD030920, DOI: https://doi.org/10.1029/2019JD030920 (2020).

[49] Bednarz, E. M. *et al.* Future Arctic ozone recovery: the importance of chemistry and dynamics. *Atmospheric Chem. Phys.* **16**, 12159–12176, DOI: 10.5194/acp-16-12159-2016 (2016).

Methods

Models

We investigate ozone feedbacks in two chemistry climate models, WACCM version 4 and SOCOL-MPIOM. WACCM (Whole Atmosphere Community Climate Model) is the atmospheric component of the NCAR Community Earth System Model version 1 (CESM1.2.2). It is a fully interactive high-top chemistry climate model [31] coupled to an active ocean [50] and sea ice components [51]. Extending to the lower thermosphere ($5.1 \cdot 10^{-6}$ hPa) in altitude with 66 vertical levels and a well resolved stratosphere [31], WACCM has been documented to capture stratospheric trends and variability reasonably well and has been used in many recent studies analysing interannual stratospheric variability (e.g., refs. [27, 33, 9] [52]). WACCM has a horizontal resolution of 1.9° latitude and 2.5° longitude [31], while the ocean has a nominal latitude-longitude resolution of 1°. Being coupled to an interactive chemistry scheme [53], WACCM calculates ozone concentrations over a set of chemical equations between a total of 59 species [31] and therefore actively simulates feedbacks between ozone and dynamics. In addition, WACCM can be run in a "specified chemistry" mode, where ozone concentrations and other radiative species are prescribed in the form of zonal mean or three-dimensional monthly or daily mean climatologies [54].

SOCOL (SOlar Climate Ozone Links) version 3 is a chemistry climate model based on the general circulation model MA-ECHAM5 and the chemistry transport model MEZON (Model for Evaluation of oZONe trends [55]), which are interactively coupled via 3-D temperature and wind fields and through radiative forcing induced by several greenhouse gases (water vapor, ozone, methane, nitrous oxide, and chlorofluorocarbons (CFCs)) [56]. MEZON includes a set of 140 gas-phase, 46 photolysis and 16 heterogeneous reactions between 41 species. SOCOL in its default configuration therefore incorporates feedbacks between ozone and dynamics. Like WACCM, SOCOL can be run in a "specified chemistry" mode through decoupling of chemistry and general circulation model, in which case ozone concentrations are prescribed as either zonal mean, monthly mean climatologies, or three-dimensional, daily mean climatologies [32]. The model version SOCOL-MPIOM used in

this study is additionally coupled to the ocean-sea-ice model MPIOM [32]. SOCOL-MPIOM has a model top of 0.01 hPa with a well resolved stratosphere and 39 vertical levels and a horizontal resolution of T31 ($3.75^\circ \times 3.75^\circ$) [56]. Despite exhibiting a cold pole bias in the stratosphere during winter [56], SOCOL has been documented to capture the annual ozone cycle and ozone trends [56] as well as stratospheric variability [32] reasonably well.

Boundary Conditions

Since both WACCM and SOCOL-MPIOM are models with fully coupled radiation, chemistry and dynamics, both models incorporate ozone-circulation feedbacks. For the study at hand, we run both models under invariant year-2000 boundary conditions with fixed, seasonally varying atmospheric greenhouse gas (GHG) concentrations including ozone depleting substances (ODSs) and a nudged quasi-biennial oscillation (QBO). Therefore, the model simulations only show very small trends (see Fig. S6 and discussion in the supplementary material). For SOCOL, GHG concentrations and ozone depleting substances (ODS) have been prescribed following the approach in Stenke et al. (2013) [56] and the QBO has been nudged according to Broennimann et al. (2007) [57]. In WACCM, a perpetual 28-month QBO cycle was forced based on the setup described in Marsh et al. (2013) [31]. Boundary conditions were prescribed following the CMIP5 forcing data sets [58].With concentrations of ODSs being set to year-2000 levels, this setup yields a high polar stratospheric ozone variability in spring and thus maximised ozone feedbacks. It also removes the effects of climate change, thereby aiding the statistical analysis.

Experiment design

To assess the impact of ozone feedbacks, we contrast runs with fully interactive and specified ozone chemistry in both models. Within the fully interactive ozone runs (INT-3D), the free running models interactively calculate ozone concentrations, therefore allowing the simulation of ozone feedbacks into the general circulation. Averaging over all 200 simulated years of INT-3D SOCOL

and INT-3D WACCM, ozone climatologies are derived and used as prescribed forcings in simulations without interactive ozone (CLIM-2D and CLIM-3D). We perform two different simulations with specified ozone chemistry: One using a zonal mean, monthly mean ozone climatology derived from INT-3D (CLIM-2D), and another one using a three-dimensional, daily mean ozone climatology from INT-3D (CLIM-3D).

For both runs with specified ozone chemistry (CLIM-3D and CLIM-2D) we use a hybrid model setup: while interactive ozone is still being calculated and saved as output, it is decoupled from the models' radiation schemes and replaced by ozone climatology from INT-3D. In this setup without interannually varying radiative ozone forcing, ozone feedbacks are not simulated; ozone thus acts as a passive tracer of dynamical variability in the stratosphere. The advantage of this setup compared to a more standard approach without any chemistry scheme is the better comparability between INT and CLIM experiments, as the oxidation of other radiatively active gases, such as CH_4, N_2O and CFCs, by ozone via $O(^1D)$, is still considered in the CLIM setting. Comparisons of CLIM experiments with runs with interactive ozone chemistry therefore allow us to draw robust conclusions about the role of ozone feedbacks in the climate system. In addition, the hybrid approach allows us in addition to apply the same definition for detecting the 25% most extreme ozone minima as for reanalysis (50 events out of 200 simulated years) in all CLIM and INT experiments. A similar set-up has already been used in the context of SH ozone depletion [59]. To account for the high interannual stratospheric variability within the system, we simulate a total of 200 model years for each of the four runs. The model setup is illustrated in Figure 3 a.

Sampling of ozone minima

Springtime ozone minima are defined based on daily zonally averaged ozone mixing ratios. To exclude outliers from being counted as "ozone minimum", a 5-day running mean of ozone mixing ratios is derived from the daily data. In order to detect the impact of ozone feedbacks, it is desirable to select the springtime ozone minima based on the altitude exhibiting the largest interannual ozone variability. Since the year-to-year ozone variance maximizes at different altitudes in WACCM, SOCOL-MPIOM and MERRA2 (see supplementary Fig. S7), we select years with springtime

ozone minima based on partial ozone column from 30-70 hPa rather than based on a specific altitude to standardize treatment of different datasets. The partial ozone column was calculated based on the 5-day running mean daily ozone mixing ratios in DU according to

$$O_{3,\mathrm{pcol}} = \frac{1\mathrm{DU}}{2.687 \cdot 10^{16} \frac{\mathrm{molec}}{\mathrm{cm}^2}} \sum_{p=30\mathrm{hPa}}^{70\mathrm{hPa}} \frac{\chi_{O_3}(p) \cdot 10 \cdot \Delta p}{g \cdot m_{\mathrm{air,d}}} \tag{1}$$

where $\chi_{O_3}(p)$ denotes the ozone mixing ratio at pressure level p, Δp describes the distance to the next pressure level in Pa, g is the gravitational constant (in $\frac{\mathrm{cm}}{\mathrm{s}^2}$ and $m_{\mathrm{air,d}}$ the mass of dry air (in $\frac{\mathrm{g}}{\mathrm{molec}}$). For each year within a dataset, the minimum polar cap mean (60-90°N) partial ozone column value within March and April is selected. For each dataset, the 25% of years with the lowest minimum partial ozone column in March and April are considered "low ozone years" (10 events in MERRA2, 50 events for each model simulation). The day at which the minimum ozone value occurs is considered the "ozone minimum date". If not stated otherwise, the data is weighted with the cosine of latitude for latitudinal averaging.

Calculation of anomalies

To calculate anomalies of a variable, a climatology for the respective variable is derived for each day of the year by averaging each calendar day over all years available in the dataset. This daily climatology is subtracted from the daily variable values to obtain daily anomalies. For MERRA2, a daily climatology is derived by averaging over the years 1980 to 2019. Since the spring in 2020 exhibited particular strong anomalies in both stratospheric and surface climate and the MERRA2 record is comparably short, the year 2020 is excluded in the calculation of the daily climatology [11].

Bootstrapping significance test

A 1-sample bootstrapping significance test is performed to estimate the significance of mean anomalies composited around the ozone minimum (e.g. [27, 33]). For a composite including the 25% most

extreme springtime ozone minima, 500 random composites are created by sampling data around the respective ozone minimum dates in random years to create a normal distribution of random composites. The actual composite is considered significantly different from zero if it differs more than 2 standard deviations from the mean of the randomly created distribution, which is equivalent to a significance at the 95.4% level. The procedure for a 2-sample bootstrapping significance test is conducted accordingly: To compare two composites, random composites are created as described above in both datasets and the difference of both random composites was calculated. Repeating this procedure 500 times, we create a distribution of 500 random samples. The difference between both samples is considered significant if it differs more than 2 standard deviations from the mean value of the random distribution.

Calculation of Arctic Oscillation and NAM indices

While the AO and NAM in general describe the same phenomenon of simultaneous fluctuations in geopotential height of opposite sign over the polar cap and lower latitudes[29], we refer to the NAM as the pattern on all vertical levels, whereas the AO is used to describe the near-surface profile at 1000 hPa [29]. Empirical Orthogonal Functions (EOFs) are used to calculate the AO and NAM indices following method 3 in Baldwin et al. (2009) [60]. For each pressure level, we calculate the leading EOF spatial pattern of year-round daily zonal mean geopotential height anomalies north of 20°N while applying latitudinal weights as the square root of the cosine of latitude [29]. Daily geopotential height anomalies are then projected onto the EOF loading pattern to find the Principal Component (PC) time series. PCs are normalized to unit variance to derive the respective AO and NAM indices.

Calculation of dynamical heating rate

We calculate the vertical ($\bar{w}^*$) and meridional ($\bar{v}^*$) component of the residual circulation according to the transformed Eulerian mean framework described by equations 3.5.1 and 3.5.2 in [61]. To examine changes in temperature induced by ozone related changes in the Brewer Dobson Circulation (BDC), we calculate the adiabatic dynamical heating in the Arctic stratosphere based on the

Quasi-Geostrophic (QG) theory according to

$$\frac{\delta \bar{T}}{\delta t} = S \cdot \bar{w}^* \tag{2}$$

where $\bar{T}$ is the zonal mean temperature and S the atmospheric stability parameter [62] which can be calculated according to Garcia et al. (2012) [63] as follows:

$$S = \frac{H \cdot N^2}{R^*}. \tag{3}$$

N^2 hereby denotes the Brunt–Väisälä frequency, H the atmospheric scale height and R^* the specific gas constant for mixed gases.

Calculation of Final Warming date

Final warmings are defined as the first date when the zonal mean wind at 60°N and 10 hPa turns easterly and does not return to westerlies for more than 10 consecutive days until the next winter [64]. Uncertainty in the final warming date is estimated based on the standard deviation.

Data availability

The modelling data used in this study is available in the ETH Research Collection. Data for WACCM: https://www.research-collection.ethz.ch/handle/20.500.11850/527155[65]. Data for SOCOL-MPIOM: https://www.research-collection.ethz.ch/handle/20.500.11850/546039 [66].

The MERRA2 reanalysis data can be downloaded from the Goddard Earth Sciences Data and Information Services Center (GES DIC) (https://disc.gsfc.nasa.gov/datasets?keywords=%22MERRA-2%22&page=1&source=Models%2FAnalyses%20MERRA-2).

Code availability

All codes and scripts used for the analysis in this study are available from the corresponding author upon reasonable request.

References

[50] Danabasoglu, G. *et al.* The CCSM4 Ocean Component. *J. Clim.* **25**, 1361 – 1389, DOI: 10.1175/JCLI-D-11-00091.1 (2012).

[51] Holland, M. M., Bailey, D. A., Briegleb, B. P., Light, B. & Hunke, E. Improved Sea Ice Shortwave Radiation Physics in CCSM4: The Impact of Melt Ponds and Aerosols on Arctic Sea Ice. *J. Clim.* **25**, 1413 – 1430, DOI: 10.1175/JCLI-D-11-00078.1 (2012).

[52] Rieder, H. E., Chiodo, G., Fritzer, J., Wienerroither, C. & Polvani, L. M. Is interactive ozone chemistry important to represent polar cap stratospheric temperature variability in Earth-System Models? *Environ. Res. Lett.* **14**, 044026, DOI: 10.1088/1748-9326/ab07ff (2019).

[53] Kinnison, D. E. *et al.* Sensitivity of chemical tracers to meteorological parameters in the MOZART-3 chemical transport model. *J. Geophys. Res. Atmospheres* **112**, DOI: https://doi.org/10.1029/2006JD007879 (2007).

[54] Smith, K. L., Neely, R. R., Marsh, D. R. & Polvani, L. M. The Specified Chemistry Whole Atmosphere Community Climate Model (SC-WACCM). *J. Adv. Model. Earth Syst.* **6**, 883–901, DOI: https://doi.org/10.1002/2014MS000346 (2014).

[55] Egorova, T., Rozanov, E., Zubov, V. & Karol, I. Model for investigating ozone trends (MEZON). *Izvestiya - Atmospheric Ocean. Phys.* **39**, 277–292 (2003).

[56] Stenke, A. *et al.* The SOCOL version 3.0 chemistry–climate model: description, evaluation, and implications from an advanced transport algorithm. *Geosci. Model. Dev.* **6**, 1407–1427, DOI: 10.5194/gmd-6-1407-2013 (2013).

[57] Brönnimann, S., Annis, J. L., Vogler, C. & Jones, P. D. Reconstructing the quasi-biennial oscillation back to the early 1900s. *Geophys. Res. Lett.* **34**, DOI: https://doi.org/10.1029/2007GL031354 (2007).

[58] Meinshausen, M. *et al.* The RCP greenhouse gas concentrations and their extensions from 1765 to 2300. *Clim. Chang.* **109**, 213–241, DOI: https://doi.org/10.1007/s10584-011-0156-z (2011).

[59] Waugh, D. W. *et al.* Effect of zonal asymmetries in stratospheric ozone on simulated Southern Hemisphere climate trends. *Geophys. Res. Lett.* **36**, DOI: https://doi.org/10.1029/2009GL040419 (2009).

[60] Baldwin, M. P. & Thompson, D. W. A critical comparison of stratosphere–troposphere coupling indices. *Q. J. Royal Meteorol. Soc.* **135**, 1661–1672, DOI: https://doi.org/10.1002/qj.479 (2009).

[61] Andrews, D. G., Holton, J. R. & Leovy, C. B. *Middle atmosphere dynamics* (Academic Press, San Diego, California, 1987).

[62] Calvo, N., Garcia, R. R. & Kinnison, D. E. Revisiting Southern Hemisphere polar stratospheric temperature trends in WACCM: The role of dynamical forcing. *Geophys. Res. Lett.* **44**, 3402–3410, DOI: https://doi.org/10.1002/2017GL072792 (2017).

[63] Garcia, R. R., Kinnison, D. E. & Marsh, D. R. "World avoided" simulations with the Whole Atmosphere Community Climate Model. *J. Geophys. Res. Atmospheres* **117**, DOI: https://doi.org/10.1029/2012JD018430 (2012).

[64] Butler, A. H. & Gerber, E. P. Optimizing the Definition of a Sudden Stratospheric Warming. *J. Clim.* **31**, 2337 – 2344, DOI: 10.1175/JCLI-D-17-0648.1 (2018).

[65] Friedel, M. & Chiodo, G. Model results for "Robust effect of springtime Arctic ozone depletion on surface climate", DOI: 10.3929/ethz-b-000527155 (2022).

[66] Friedel, M. & Chiodo, G. Model results for "Robust effect of springtime Arctic ozone depletion on surface climate", part 2. Data for SOCOL-MPIOM, DOI: 10.3929/ethz-b-000546039 (2022).